ACS APPLIED MATERIALS & INTERFACES

Energy, Environmental, and Catalysis Applications

Sulfur Doped TiO2 Anchored on a Large-Area Carbon Sheets as High-performance Anode for Sodium-ion Battery

Yan Zhang, Xinrui He, Jiahui Tang, Jing Jiang, Xiaobo Ji, and Chao Wang

ACS Appl. Mater. Interfaces, **Just Accepted Manuscript** • DOI: 10.1021/acsami.9b14597 • Publication Date (Web): 01 Nov 2019

is published by the American Chemical Society. 1155 Sixteenth Street N.W., Washington, DC 20036

Sulfur Doped TiO_2 Anchored on a Large-Area Carbon Sheets as High-performance Anode for Sodium-ion Battery

Yan Zhang [a,b,c], *Xinrui He* [a], *Jiahui Tang* [d], *Jing Jiang* [a], *Xiaobo Ji* [b,e], *and Chao Wang* [a,*]

[a] Clean Energy Materials and Engineering Center, State Key Laboratory of Electronic Thin Films and Integrated Devices, School of Electronic Science and Engineering University of Electronic Science and Technology of China, Chengdu, 611731, China.

[b] College of Chemistry and Chemical Engineering, Central South University, Changsha, 410083, China.

[c] Department of Chemistry, University College Cork, Cork, T12 K8AF, Ireland.

[d] School of Minerals Processing and Bioengineering, Central South University, 410083, China

[e] School of Metallurgy and Chemical Engineering, Jiangxi University of Science and Technology, Ganzhou, 341000, China.

KEYWORDS: Sodium-ion battery; Anode; Titanium dioxide; Sulfur doped; Carbon sheets; electrochemical performance; pseudocapacitance behavior.

ABSTRACT: A well-tailored sulfur-doped anatase titanium dioxide nanoparticles anchored on a large-area carbon sheets are designed, where the in-situ sulfur doped titanium dioxide directly comes from titanium oxysulfate, and the large-area carbon sheets derive from glucose. When applied as anode material for sodium-ion batteries, it exhibits an excellent electrochemical performance including a high capacity (256.4 mAh g^{-1} at 2 C (1 C=335 mAh g^{-1}) after 500 cycles) and a remarkable rate cycling stability (100.5 mAh g^{-1} at 30 C after 500 cycles). These outstanding sodium storage behaviors are ascribed to nanosized particles (about 8-12 nm), good electronic conductivity promoted by the incorporation of carbon sheets and sulfur, as well as the unique chemical bond based on electrostatic interaction.

1. INTRODUCTION

Currently, sodium-ion batteries (SIBs) are considered as the most appealing candidate power sources to lithium-ion batteries (LIBs) due to more abundant sodium resources in the earth crust (Na: 23600 ppm; Li: 20 ppm) and much lower price (Sodium carbonate: 0.07-0.37 € kg^{-1}; Lithium carbonates: 4.11-4.49 € kg^{-1}).[1-6] It is also proposed that the electrode materials of LIBs are introduced as those of SIBs on the basis of their similar working principles.[7] However, given that a larger radius (Na^+: 1.02 Å; Li^+: 0.76 Å) and less electronegative nature of sodium (Na^+/Na: -2.71 V (vs. SHE); Li^+/Li: -3.04 V (vs. SHE)),[8-10] there is a narrower alternative pool of cathode and anode electrode materials for SIBs.[11-14] For example, the graphitic carbon, as an ideal anode for commercial LIBs, is proved a low specific capacity of 31 mAh g^{-1},

corresponding to the formation of NaC_{70} in the electrochemical sodiation process.[15-19] Thus, titanium oxide (TiO_2) has been considered as one of the most potential anodes for SIBs because of high theoretical specific capacity of 335 mAh g^{-1}, the diversity of crystal as well as earth abundance. In addition, the chemical stability, environmental benignity and low insertion potential (about 0.8 V) of TiO_2 is also greatly helpful toward large-scale applications.[20-24] But the rate capabilities of TiO_2 are limited by its sluggish intercalation kinetics and poor electron mobility in bulk materials.

Amounts of attempts have been made to promote the diffusion kinetics of sodium ion and improve the intrinsic electronic conductivity of TiO_2, where downsizing the particles,[25-27] the encapsulation of carbon,[28-31] the loading of graphene[32] and the incorporation of hetero elements[33-37] are regarded as the most common strategies. For instance, carbon coating TiO_2 nanoparticles with the size of 11 nm were proved to deliver a robust capacity of 134 mAh g^{-1} at a rate of 10 C (3350 mA g^{-1}). F-doped anatase TiO_2/CNT composite exhibited a reversible charge-discharge capacity of approximately 90 mAh g^{-1} at a current density of 35 C (8750 mA g^{-1}).[38] The brilliant high-rate performances were presented in nitrogen-doped yolk-like anatase TiO_2/C composite (a reversible capacity of 116 mAh g^{-1} at 20 C),[39] and graphene-rich wrapped petal-like rutile TiO_2 composites (a reversible capacity of 74.6 mAh g^{-1} at 10 C)[32]. These adequately demonstrated that the above methods are extremely effective to solve the drawback of TiO_2 and obviously improve its sodium storage performance.

Additionally, pseudocapacitive sodium storage mode is introduced to improve high-rate cycling life for TiO_2 anode. For example, Chen and co-workers reported that

pseudocapacitive Na^+ ions storage behaviour enabled by the unique chemically bonded graphene-coupled TiO_2 sandwich-like hybrid with an ultra-fast sodium storage process.[40,41] It was also found that high pseudocapacitive contributions resulted from the combination of graphene-TiO_2 mesoporous structure and 3D titania-graphene hybrid.[42,43] Recently, Ji and Yu group had demonstrated that Ti^{3+} and oxygen vacancy defects can enhance pseudocapacitive behaviour in SIBs.[44,45] Thereby, it can be a good guide to improve sodium storage performances based on the synergistic effect of the chemical bond correlation, tailor-designed nanostructure and the introduction of conductive materials.

Herein, sulfur-doped anatase TiO_2 nanoparticles anchored on a large-area carbon sheets (termed as S-TiO_2/CS) is proposed, which was applied as an anode in SIBs. The successful introduction of sulfur species directly derived from titanium oxysulfate is more effective, more simplified and safer than using other sulfur powders/resource or hazardous H_2S gas. And the lower electronegativity of sulfur (in comparison with oxygen) and the less ionic nature of Ti-S (in comparison with Ti-O) may shrink bandgap energy and improve the electrical conductivity of TiO_2.[46] Notably, the strong connections between TiO_2 and conductive substrate induced by the electrostatic interaction are greatly beneficial to sodium ion intercalation in bulk TiO_2 crystal and the pseudocapacitive sodium storage in the surface/interface.[43] Furthermore, the combination of with carbon sheets and sulfur doping aimed at drastically boosting electronic transfer. Synergistically, the ultrafine nanoparticles can shorten sodium ion diffusion distance which could facilitate electrochemical kinetics.

2. EXPERIMENTAL SECTION

2.1 Preparation of the S-TiO_2/CS composites.

All reagents were of analytical grades and used without further purification. In a typical prepared progress, 2.0 g of titanium oxysulfate ($TiOSO_4$, >99.7%, Sigma-Aldrich) were dissolved in 40 mL of isopropyl alcohol (IPA, >99.7%, Sigma-Aldrich) with vigorously stirring for 0.5 h. Subsequently, 0.03 mL of diethylenetriamine (DETA, >99%, Sigma-Aldrich) and 0.1 g glucose (99%, Alfa Aesar) were added into above uniform solution. When the reaction was finished, as-obtained products were washed with ethanol and deionized water for several times via centrifugation, and then dried in vacuum oven at 80 °C for overnight. The S-TiO_2/CS composites were synthesized after annealing in a tube furnace at 800 °C for 2 h in argon atmosphere.

2.2 Materials characterization

The X-ray diffraction (XRD) patterns were recorded via using a Rigaku D/max 2550 VB+ 18 kW diffractometer (Japan) with Cu Kα radiation (λ=1.542 Å), which were used to confirm the crystalline structures of S-TiO_2/CS composites. The field emission scanning electron microscopy (FESEM) images were obtained with a FEI Quanta 200 instrument (Japan), and the transmission electron microscopy was conducted on a JEOL JEM-2100F electron microscopy (Japan), which was aimed at observing the morphologies of S-TiO_2/CS samples. X-ray photoelectron spectroscopy (XPS) was performed on a K-Alpha 1063 instrument (UK). The Brunauer-Emmett-Teller (BET, BELSORP-MINI II) specific surface area was

calculated according to the nitrogen adsorption-desorption curves at 77K. The pore size distribution was determined on the basis of the Barrett-Joyner-Halenda (BJH) method.

2.3 Electrochemical measurements

The S-TiO_2/CS electrode was prepared as below: the mixed slurries were made up of 70 wt% of as-prepared active material (S-TiO_2/CS composites), 15 wt% of conductive additive (Super P, >99%, Alfa Aesar) and 15 wt% of binder (polyvinylidene fluoride, PVDF, Alfa Aesar), which were uniformly painted on a copper foil. After drying, it was punched into wafers and used as the anode for SIBs. The average mass loading of the wafers was approximately 1.2-1.5 mg cm^{-2}. The sodium storage performance was estimated by CR2016-type coin cells, where the sodium metal was acted as the counter electrode, the Celgard 2400 polyethylene was used as the separator. And the electrolyte was consisted of 1 M sodium perchlorate ($NaClO_4$, >99%, Alfa Aesar) dissolving in solvent of propylene carbonate (PC, >99.7%, Alfa Aesar) and fluoroethylene carbonate (FEC, >99%, Alfa Aesar) additive (the volume ratio of 95:5). The half cells were assembled in an argon-filled glovebox (mBraun, Germany) where water/oxygen content is lower than 1 ppm. The cyclic voltammetry (CV) data were recorded on Solartron Analytical (Ametek, UK). The Galvanostatic charge-discharge cycling and rate performance analysis were carried out on a LAND cycler (Wuhan Kingnuo Electronic Co., China) and Arbin battery cycler (BT 2000, USA). All the cell tests were performed in a voltage range between 0.01 and 3.0 V (vs. Na^+/Na).

3. RESULTS AND DISCUSSION

3.1 Morphology and structure

As shown in the XRD patterns (Fig. 1), the sharp identified peaks observed at 25.25°, 37.81°, 48.08°, 53.85°, 55.16°, 62.78°, 68.67°, 70.38° and 75.03° can be assigned to (101), (004), (200), (105), (211), (204), (116), (220) and (215) crystal faces of tetragonal anatase TiO_2 (a space group of I41/amd) according to the JCPDS card 21-1272. Additionally, there is no impurity peak resulting from other secondary phases, suggesting the presence of highly pure anatase TiO_2 phase.

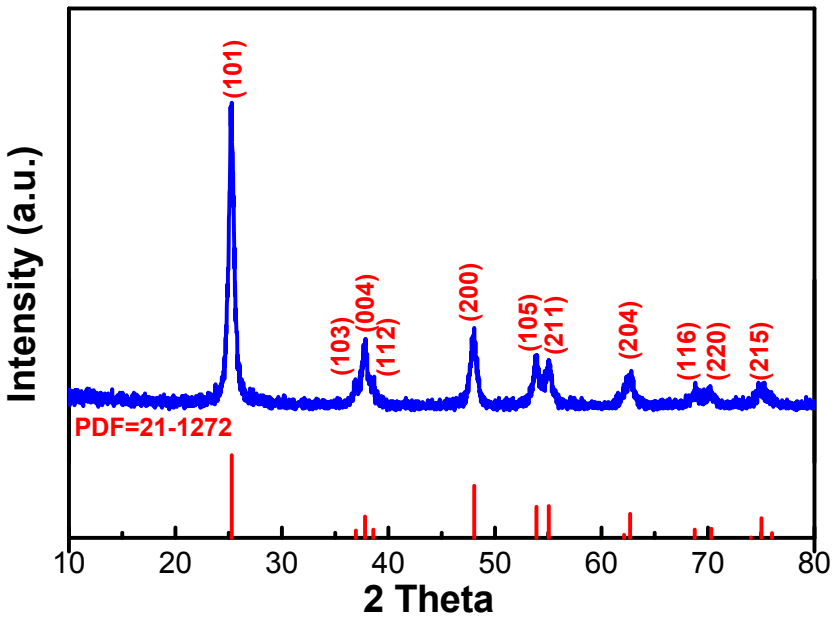

Fig.1. XRD images of the as-prepared S-TiO_2/CS composites.

The structural and morphological properties of S-TiO_2/CS sample are confirmed by scanning electron microscopy (SEM) and transmission electron microscopy (TEM). As displayed in Fig. 2a and b, plenty of tiny nanograins are captured on both sides of sheets, which are ultra-large in size and rather thin. And the wrinkle/rough surfaces and porous feature might be distinctly identified through the SEM images at

a higher magnification (Fig. 2c and d) and a typical TEM image in Fig. 2e. Interestingly, the enlarged TEM images (Fig. 2f and g) show that unique nanograins anchored in folded microsheet architecture composed of numerous nanoparticles with a size of 8-12 nm. It can also clearly observe that nanograins are the irregularity shape feature. As shown in the high-resolution TEM image (Fig. 2h), it displays a set of parallel lattices with spacing of 0.35 nm, corresponding to the (101) lattice plane of anatase TiO_2. The nanoparticles with a size of 8-12 nm might be helpful to shorten the ion diffusion paths, and the structural porosity may facilitate sodium ion diffusion. The large-area thin sheets substrate with wrinkle feature can be beneficial to interfacial reaction and electrolyte wetting.

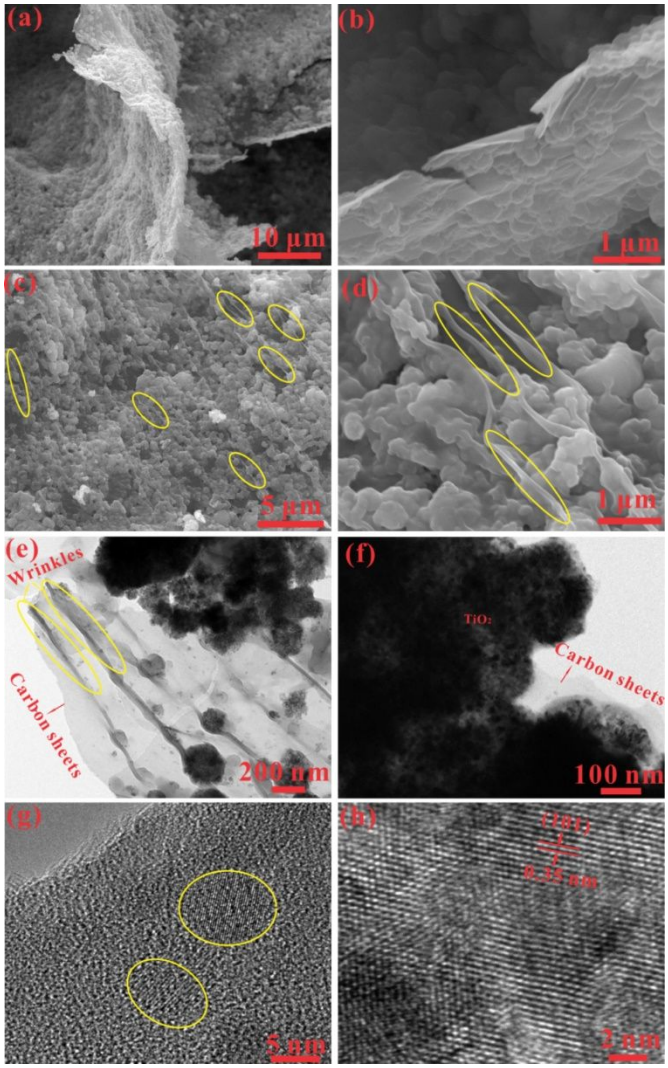

Fig. 2. (a-d) FESEM image and (e-h) TEM image of the S-TiO_2/CS composites.

The specific surface area and the pore size distribution are determined by the nitrogen adsorption-desorption measurement. As displayed in Fig. 3a, there is a distinct hysteresis loop appeared at high pressures in the N_2 adsorption-desorption isotherms, which indicates a type IV isotherm characteristic of H3 hysteresis loop. According to BET measurement, the specific surface area of the S-TiO_2/CS composites is 181.95 m^2 g^{-1}. Meanwhile, based on BJH method, it confirms narrow pore with size distribution of 3.965 nm (Fig. 3b), demonstrating the mesoporous structure of the material, which resulted from the wrinkle surfaces of sheets and

between nanograins.[47] The high specific surface area accompanied with mesoporous feature could be greatly helpful to more active sites of sodium storage and increase the wetting areas of electrolytes, accelerating kinetic reaction between the TiO_2 electrodes and sodium ion.

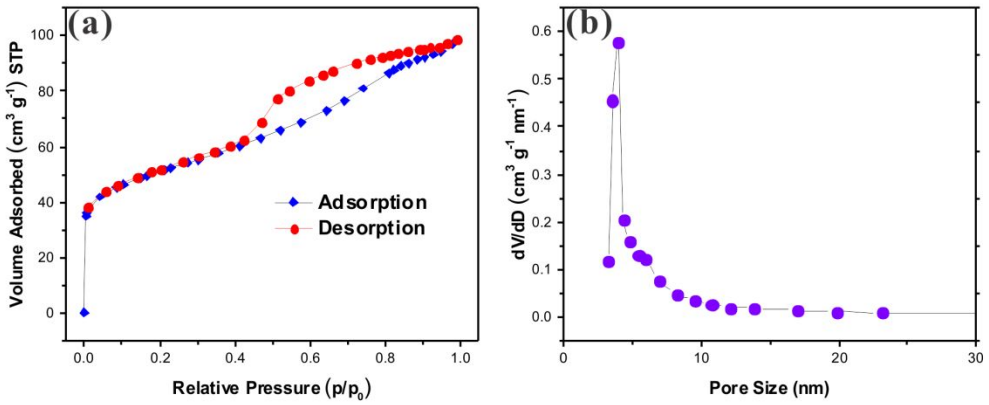

Fig. 3. (a) Nitrogen adsorption-desorption isotherms and (b) the corresponding BJH pore size distribution of the S-TiO_2/CS composites.

To analysis the chemical state of as-prepared S-TiO_2/CS composites, XPS spectrum of samples, Ti 2p, S 2p, and C 1s were performed. As exhibited in Fig. 4a, typical TiO_2 spectra and obvious S, N, and C peaks are identified, eliminating the presentence of other impurities. The obvious Ti 2p peak at 458.56 eV as well as a weaker peak at 464.24 eV are the typical signals of Ti $2p_{3/2}$ and Ti $2p_{1/2}$ of the tetravalent Ti ion species, respectively (Fig. 4b).[48] The chemical state of sulfur was verified by the S2p core level XPS pattern in the Fig. 4c, where was fitted in several peaks. The intense peaks at binding energies (BEs) of 163.23 eV and 164.29 eV can be assigned to the $S2p_{3/2}$ and $S2p_{1/2}$ of the sulfide group (-C-S_x-C-, x = 1-2).[49] Two extra intense XPS peaks appear at a higher BE (166.12 and 168.35 eV) are associated

with the existence of doped S element,[50-52] which strongly suggested that the sulfur is possibly covalently bonded with carbon and successfully incorporated into TiO_2. Note that S content close to 4% and the percentage of TiO_2 is about 50% according to the XPS data. Additionally, the small split separately occurred at 161.64 eV corresponds to anionic S^{2-} species, which is also in good agreement with previous reports.[46] In the case of C1s (Fig. 4d), the feature of carbon mainly appear at 284.81 (C-C/C-S), 285.99 (C-O/C-S), 286.94 (C=O), 288.54 (-CO^{2-}) and 291.29 eV (π-π*).[37,53,54] More significantly, the peak at 283.79 eV can be assignable to C-Ti covalent bond[40,55] and the peaks at 284.81 and 285.99 eV could be ascribed to the C-S bridge bond.[56,57]

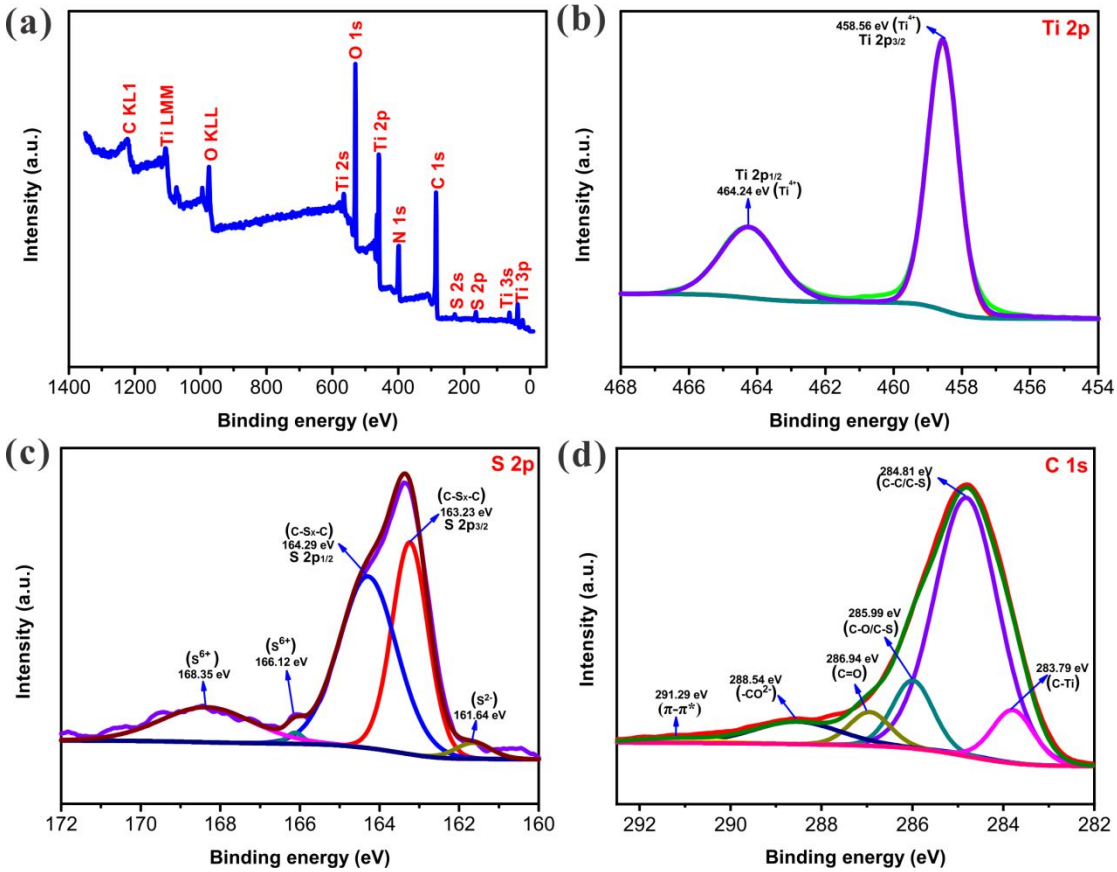

Fig. 4. . (a) Integrated XPS spectrum and high-resolution XPS spectra of (b) Ti2p, (c) S2p, (d) C1s of the S-TiO_2/CS composites.

Notably, taking into account the formation of a covalent bond between the S, Ti and C, it indicates that there is a unique chemical attachment between S-doped TiO_2 and large-area carbon sheets conductive substrate, rather than simple adhesion connection. These strongly chemically combined interactions can provide the coherent pathway for electron transfer and ion transmission, which is beneficial to the fast charge-discharge process. On the other hand, it can also lead to more interfacial pseudocapacitive sodium storage performance, which is responsible for high rate long-term cycling life.

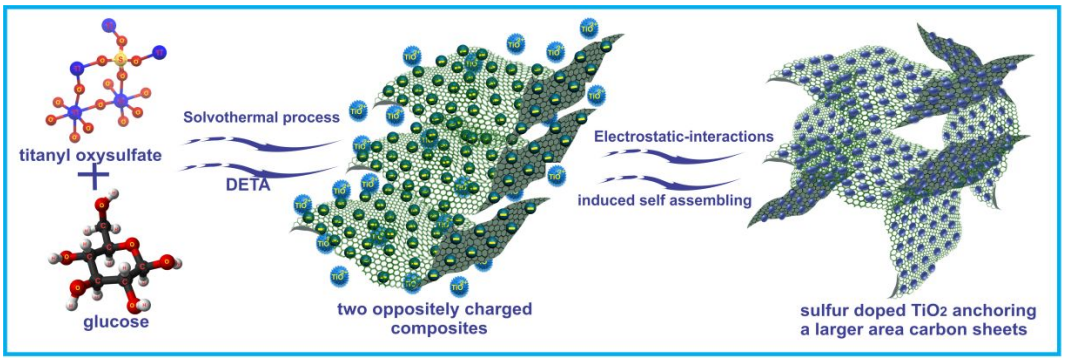

Fig. 5. Schematic illustration of the S-TiO_2/CS composites.

An "electrostatic-interaction-induced self-assembling" can be introduced as the formation mechanism of S-TiO_2/SC.[43,58] As displayed in Fig. 5, titanium oxysulfate, as a titanium source, is in the form of $(TiO)_n^{2n+}$ polymerized by TiO^{2+} in the isopropyl alcohol solution, directly exhibiting a positive surface charges. During the solvothermal reaction process, glucose prefers to produce some aromatic composites, which mostly possessing a high amount of multiple hydroxyl groups.[59-61] Thus, these hydroxyl functional groups can serve as anchoring bridge to strongly connect positively titanium source and carbon sheets by π-π* interactions, which cannot be

similar to commonly reported methods through directly adding graphene nanosheets or aced-assisted CNT.[43] [62,63] Compared to the van der Waals forces inducing the connection of active materials and carbon substrates, the electrostatic-interaction between two oppositely charged reaction composites can induce a strongly driving force through self-assembling, and further form interface by the unique chemical bond. As for S-TiO_2/CS, the cooperation effects of sulfur doping and large-area carbon sheets substrate can provide a coherent electronic transfer path, which is helpful to fast electron and sodium ion transportation. The strong interaction between large-area carbon sheet and tiny TiO_2 nanoparticles can have a great improvement of the pseudocapacitive sodium storage, which is significantly crucial for high rate long-term cycle life.

3.2 Electrochemical performance

The cyclic voltammograms (CVs) of as-obtained S-TiO_2/CS electrode are performed at a scan rate of 0.1 mV s^{-1} in Fig. 6a, which displays a characteristic electrochemical feature of anatase TiO_2. In the initial cathodic scan, two irreversible peaks are observed at around 0.48 V and 1.01 V, which is assigned to the formation of solid electrolyte interface layer and some parasitic side reactions of electrolyte.[64] Additionally, a small peak at approximately 0.87 V appears, suggesting the reversible reduction between tetravalent and trivalent of titanium ion. In all anodic sweeps, the peak at 0.89 V is reserved, which indicates reversible oxidation of TiO_2. Meanwhile, the CVs curves and a pair of redox peaks almost overlap from second to fifth cyclic scan, further pointing out that high reversibility of TiO_2 reacted with sodium ion. The

discharge-charge curves at a current density of 0.5 C (Fig. 6b) also verify similar phenomenon, where the charge profiles overlap well, whereas the profiles vary in the initial three discharge process. Accompanied with discharge-charge process at different rates (Fig. 6c), it can be observed that a wide plateau at 0.7-1.0 V in discharge period and a broad plateau at 1.0-1.3 V in charge period are maintained, significantly manifesting reversible insertion-extraction of Na^+ ions.

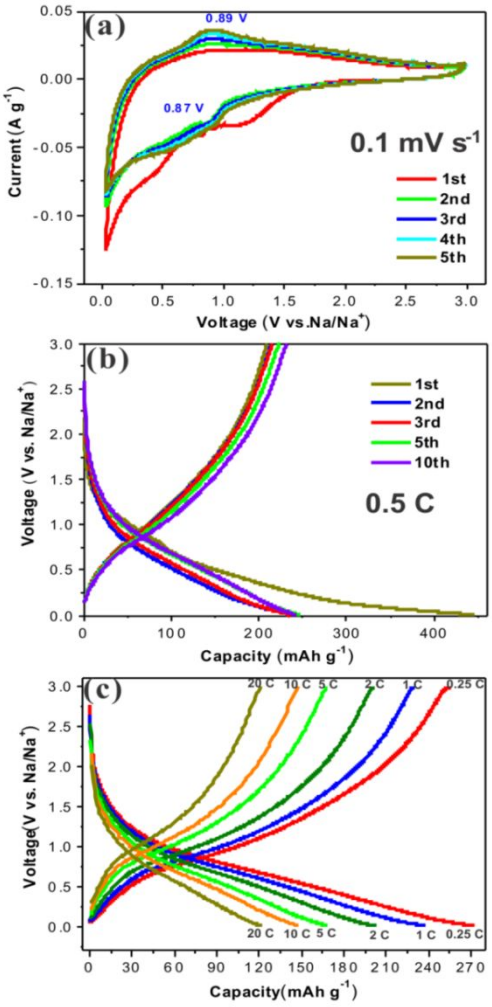

Fig. 6. (a) CV curves at a scan rate of 0.1 mV s^{-1}, (b) charge-discharge profiles of the first, second, third, fifth and tenth cycle at a current density of 0.5 C, (c) charge-discharge profiles at different rate for the S-TiO_2/CS composites anode.

The galvanostatic discharge-charge tests at current densities of 0.5 C and 2 C are depicted in Fig. 7a and b, respectively. In the first cycles, the moderate discharge capacities of 445.6 (0.5 C) and 317.6 mAh g^{-1} (2 C) are delivered, whereas the relatively small charge capacities of 209.4 (0.5 C) and 140.7 mAh g^{-1} (2 C) are yielded, corresponding to low Coulombic Efficiencies of 47% (0.5 C) and 44.3% (2 C). The large capacity loss and inferior initial Coulombic Efficiency might mainly derive from some side reactions between TiO_2 surface and the electrolyte as well as some irreversible reduction from TiO_2 to metallic titanium and sodium superoxide,[64] which would resolve through the pre-sodiation technique in term of the practical application. And a trend of gradually increasing capacity over first 25 cycles can be seen at different current densities, resulting from the activation phenomenon of electrode,[65] which is also coincident with the CV tests where the current density of anodic peak keeps rising with the number of times sweeping increasingly. During repeated cycles, the specific capacities of 293.5 (0.5 C) and 256.4 mAh g^{-1} (2 C) are retained, reflecting an excellent cycle performance. Note that Coulombic Efficiency significantly goes up in the 10^{th} cycle, and then rose smoothly to 99% and keep at the level in following cycles.

Fig. 7c presents superior rate performance of S-TiO_2/CS electrodes, the specific capacities of 255.5, 228.6, 200.8, 167.6, 146.5 and 120.6 mAh g^{-1} are achieved at rate of 0.25, 1, 2, 5, 10 and 20 C, respectively. Even at 20 C, it can still deliver a high capacity of about 120 mAh g^{-1} after 655 cycles, exhibiting a robust tolerance during fast sodium ion inserting into/extracting out process. More excitingly, at higher

current density of 30 C, a surprising capacity of 100.5 mAh g^{-1} is obtained for 5000 cycles (Fig. 7d), further revealing that the S-TiO_2/CS electrodes possess a high-rate long-term cyclability, which is a crucial but challenging factor for an attractive anode in future commercial batteries.

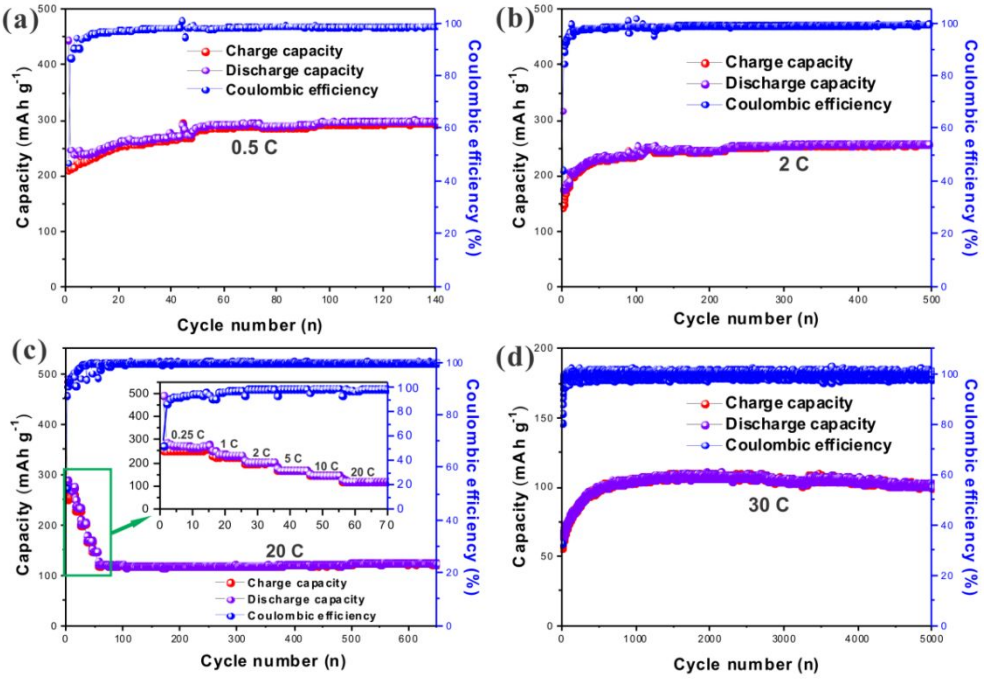

Fig. 7. (a) Cycle performances at a rate of 0.5 C for 140 cycles, (b) cycle performances at a rate of 0.5 C for 500 cycles, (c) rate capability at different current densities, (d) high-rate long-term cycle life at a rate of 30 C for the S-TiO_2/CS composites anode.

The kinetics process of sodium storage for S-TiO_2/CS electrode is investigated by CV tests at various sweep rates ranging from 0.1 to 100 mV s^{-1}. As displayed in Fig. 8a and b, it can be seen that a pair of broad redox peaks are almost reserved at the scan rate of 0.1-30 mV s^{-1}. And when sweep rate exceeds 40 mV s^{-1} (Fig. 8c), there

undergoes a distinctly distortion because of the polarization of electrode. Meanwhile, the current value (*i*) of peak becomes large with increasing sweep rate (*v*). A power-law equation ($i = av^b$) between the peaks current and sweep rate is used for studying difference in kinetics.[40,42,66,67] By mean of plotting log(*i*) against log(*v*), it can be equivalent to the relationship: log(*i*)= log(*a*)+ *b*log(v), where *i* and *v* are acknowledged form experimental tests, *a* and *b* are determined by fitting method. Generally, b value closes to 1 corresponds to the capacitive-controlled electrochemical behaviour, also namely surface Faradic redox reaction, whereas b closes to 0.5, standing for a diffusion-controlled process. Fig. 8d reflects the linear relation according to b value from the slope. b value of 0.792 reveals that the dominant electrochemical process is pseudocapacitive behaviour at relatively slow sweep rates scope (<20 mV s^{-1}).

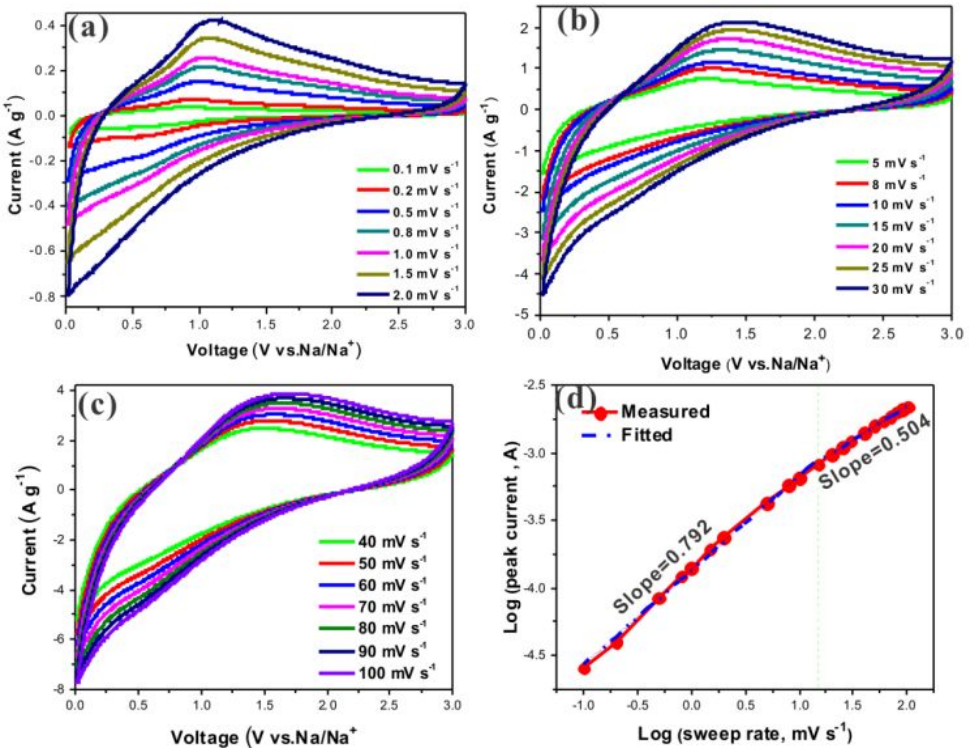

Fig. 8. CV curves at various scan rates, (a) from 0.1 to 2.0 mV s^{-1}, (b) from 5 to 30 mV s^{-1}, (c) from 40 to 100 mV s^{-1}, (d) the relationship between the peak currents and scan rates in logarithmic format for the S-TiO_2/CS composites anode.

When a certain fast scan rate (>30 mV s^{-1}), b value changes to 0.504, indicating that rate-limiting step is mainly determined by ion diffusion. Note that total sodium storage capacity of the S-TiO_2/CS electrode comes from two contributions of pseudocapacitance controlled (the interfacial Faradic redox reaction) and diffusion-controlled (a redox reaction between Ti^{4+}/Ti^{3+}), the dominating pseudocapacitive mechanism is responsible for excellent high-rate performance of the S-TiO_2/CS electrode.[42,43]

The outstanding sodium storage of the S-TiO_2/CS composite can be ascribed to the significant synergism effects of a structure design and a chemically bonded correction. The TiO_2 nanograins consisting of nanoparticles with a size of 8-12 nm anchored on carbon sheets that may shorten the ions' transport pathways and possess a high capable of reversibly accommodating sodium in the bulk. The combination of sulfur-doping and large-area carbon sheets can highly improve electronic conductivity of TiO_2, resulting in much faster electronic charge transfer and the enhanced kinetics of sodium storage process. More importantly, the strong chemical bond hybrid inducing by electrostatic interaction between the TiO_2 and carbon sheets can be beneficial to more feasible paths for sodium ion diffusion in the S-TiO_2/CS interface, which leads to accelerating sodium storage pseudocapacitive process. And the

kinetics analysis also demonstrated pseudocapacitive behaviour, which is markedly responsible for high-rate performance and rapid sodium storage process.

4. CONCLUSIONS

In summary, in-situ synthesis sulfur-doped TiO_2 nanoparticles anchored on a large-area carbon sheets are proposed by directly using titanium oxysulfate as titanium source, diethylenetriamine as complexing agent and glucose as carbon precursor, which based on an "electrostatic-interaction-induced self-assembling" mechanism. When applied as anodes for SIBs, the reversible capacities of the S-TiO_2/CS electrode are as high as 293.5 mAh g^{-1} (0.5 C) and 256.4 mAh g^{-1} (2 C). And the specific capacity of 120.6 mAh g^{-1} at a high rate of 20 C is obtained, demonstrating an impressive rate performance. More encouragingly, an ultra-long cycling stability is displayed at extra current density of 30 C for over 5000 cycles, representing the potential application in the future. The kinetic investigation reveals that the sodium ion intercalation pseudocapacitive mechanism is greatly helpful to the outstanding sodium-storage performance especially high-rate cycle life. Furthermore, the superior electrochemical properties for the S-TiO_2/CS composites can be also ascribed to the cooperation impacts of nanoparticles size, giant doping effect, robust chemical bond medication as well as a large carbon sheets conductive substrate.

AUTHOR INFORMATION

Corresponding Author

* Email address: cwang@uestc.edu.cn.

ACKNOWLEDGMENT

This work is funded by the National Natural Science Foundation of China (No. 51672037, 61727818, 61604031, 51622406, 21673298 and 21473258), the Department of science and technology of Sichuan Province (2019YFH0009), the subproject of the National Key and Development Program of China (2017YFC0602102), Project of Innovation Driven Plan in Central South (2017CX004), Hunan Provincial Science and Technology Plan (2017TP1001).

REFERENCES

(1) Lee, M.; Hong, J.; Lopez, J.; Sun, Y.; Feng, D.; Lim, K.; Chueh, W. C.; Toney, M. F.; Cui, Y.; Bao, Z.: High-performance sodium–organic battery by realizing four-sodium storage in disodium rhodizonate. *Nature Energy* **2017**, *2*, 861-868.

(2) Luo, W.; Shen, F.; Bommier, C.; Zhu, H.; Ji, X.; Hu, L.: Na-ion Battery Anodes: Materials and Electrochemistry. *Acc. Chem. Res.* **2016**, *49*, 231-240.

(3) Hwang, J.-Y.; Myung, S.-T.; Sun, Y.-K.: Sodium-ion Batteries: Present and Future. *Chem. Soc. Rev.* **2017**, *46*, 3529-3614.

(4) Wang, L.; Wang, Z.; Xie, L.; Zhu, L.; Cao, X.: ZIF-67-Derived N-Doped Co/C Nanocubes as High-Performance Anode Materials for Lithium-Ion Batteries. *ACS Appl. Mater. Interfaces* **2019**, *11*, 16619-16628.

(5) Zhu, L.; Wang, Z.; Wang, L.; Xie, L.; Li, J.; Cao, X.: ZnSe embedded in N-doped Carbon Nanocubes as Anode Materials for High-performance Li-ion Batteries. *Chem. Eng. J.* **2019**, *364*, 503-513.

(6) Wu, M.; Xu, B.; Zhang, Y.; Qi, S.; Ni, W.; Hu, J.; Ma, J.: Perspectives in Emerging Bismuth Electrochemistry. *Chem. Eng. J.* **2020**, *381*, 122558.

(7) Zhu, L.; Ding, G.; Liu, J.; Liu, Z.; Xie, L.; Cao, X.: Graphene-wrapped

poly(2,5-dihydroxy-1,4-benzoquinone-3,6-methylene) Nanoflowers as Low-cost and High-performance Cathode Materials for Sodium-ion Batteries. *Int J Energy Res.* **2019**, DOI: 10.1002/er.4764.

(8) Fang, C.; Huang, Y.; Zhang, W.; Han, J.; Deng, Z.; Cao, Y.; Yang, H.: Routes to High Energy Cathodes of Sodium-Ion Batteries. *Adv. Energy Mater.* **2016**, *6*, 1501727.

(9) Wang, C.; Tian, H.; Jiang, J.; Zhou, T.; Zeng, Q.; He, X.; Huang, P.; Yao, Y.: Facile Synthesis of Different Morphologies of Cu_2SnS_3 for High-Performance Supercapacitors. *ACS Appl. Mater. Interfaces* **2017**, *9*, 26038-26044.

(10) Cui, Z.; Li, C.; Yu, P.; Yang, M.; Guo, X.; Yin, C.: Reaction Pathway and Wiring Network Dependent Li/Na Storage of Micro-sized Conversion Anode with Mesoporosity and Metallic Conductivity. *J. Mater. Chem. A* **2015**, *3*, 509-514.

(11) Wang, Q.; Zhao, C.; Lu, Y.; Li, Y.; Zheng, Y.; Qi, Y.; Rong, X.; Jiang, L.; Qi, X.; Shao, Y.; Pan, D.; Li, B.; Hu, Y.-S.; Chen, L.: Advanced Nanostructured Anode Materials for Sodium-Ion Batteries. *Small* **2017**, *13*, 1701835.

(12) Lao, M.; Zhang, Y.; Luo, W.; Yan, Q.; Sun, W.; Dou, S. X.: Alloy-Based Anode Materials toward Advanced Sodium-Ion Batteries. *Adv. Mater.* **2017**, *29*, 1700622.

(13) Qi, S.; Xu, B.; Tiong, V. T.; Hu, J.; Ma, J.: Progress on Iron Oxides and Chalcogenides as Anodes for Sodium-ion Batteries. *Chem. Eng. J.* **2020**, *379*, 122261.

(14) Xu, B.; Qi, S.; He, P.; Ma, J.: Antimony- and Bismuth-Based Chalcogenides for Sodium-Ion Batteries. *CHEM-ASIAN J.* **2019**, *14*, 2925-2937.

(15) Doeff, M. M.; Ma, Y.; Visco, S. J.; De Jonghe, L. C.: Electrochemical Insertion of Sodium into Carbon. *J. Electrochem. Soc.* **1993**, *140*, L169-L170.

(16) Hou, H.; Banks, C. E.; Jing, M.; Zhang, Y.; Ji, X.: Carbon Quantum Dots and Their Derivative 3D Porous Carbon Frameworks for Sodium-Ion Batteries with Ultralong Cycle Life. *Adv. Mater.* **2015**, *27*, 7861-7866.

(17) Hou, H.; Shao, L.; Zhang, Y.; Zou, G.; Chen, J.; Ji, X.: Large-Area Carbon Nanosheets Doped with Phosphorus: A High-Performance Anode Material for

Sodium-Ion Batteries. *Adv. Sci.* **2017**, *4*, 1600243.

(18) Wu, T.; Zhang, C.; Zou, G.; Hu, J.; Zhu, L.; Cao, X.; Hou, H.; Ji, X.: The Bond Evolution Mechanism of Covalent Sulfurized Carbon during Electrochemical Sodium Storage Process. *Sci. China Mater.***2019**, *62*, 1127-1138.

(19) Ge, P.; Hou, H.; Cao, X.; Li, S.; Zhao, G.; Guo, T.; Wang, C.; Ji, X.: Multidimensional Evolution of Carbon Structures Underpinned by Temperature-Induced Intermediate of Chloride for Sodium-Ion Batteries. *Adv. Sci.* **2018**, *5*, 1800080.

(20) Mei, Y.; Huang, Y.; Hu, X.: Nanostructured Ti-based Anode Materials for Na-ion Batteries. *J. Mater. Chem. A* **2016**, *4*, 12001-12013.

(21) Yan, D.; Pan, L.: A New Sodium Storage Mechanism of TiO_2 for Sodium Ion Batteries. *Inorg. Chem. Front.* **2016**, *3*, 464-468.

(22) Wang, Q.; Zhao, C.; Lu, Y.; Li, Y.; Zheng, Y.; Qi, Y.; Rong, X.; Jiang, L.; Qi, X.; Shao, Y.; Pan, D.; Li, B.; Hu, Y.-S.; Chen, L.: Advanced Nanostructured Anode Materials for Sodium-Ion Batteries. *Small* **2017**, *13*, 1701835.

(23) Ge, M.; Cao, C.; Huang, J.; Li, S.; Chen, Z.; Zhang, K.-Q.; Al-Deyab, S.; Lai, Y.: A Review of One-dimensional TiO_2 Nanostructured Materials for Environmental and Energy Applications. *J. Mater. Chem. A* **2016**, *4*, 6772-6801.

(24) Zhao, L.; Wang, S.; Pan, F.; Tang, Z.; Zhang, Z.; Zhong, S.; Zhang, J.: Thermal Convection Induced TiO_2 Microclews as Superior Electrode Materials for Lithium-ion Batteries. *J. Mater. Chem. A* **2018**, *6*, 11688-11693.

(25) Zhou, M.; Xu, Y.; Wang, C.; Li, Q.; Xiang, J.; Liang, L.; Wu, M.; Zhao, H.; Lei, Y.: Amorphous TiO_2 Inverse Opal Anode for High-rate Sodium Ion Batteries. *Nano Energy* **2017**, *31*, 514-524.

(26) Li, Y.; Wang, S.; He, Y.-B.; Tang, L.; Kaneti, Y. V.; Lv, W.; Lin, Z.; Li, B.; Yang, Q.-H.; Kang, F.: Li-ion and Na-ion Transportation and Storage Properties in Various Sized TiO_2 Spheres with Hierarchical Pores and High Tap Density. *J. Mater. Chem. A* **2017**, *5*, 4359-4367.

(27) Qiu, S.; Xiao, L.; Ai, X.; Yang, H.; Cao, Y.: Yolk-Shell TiO_2@C

Nanocomposite as High-Performance Anode Material for Sodium-Ion Batteries. *ACS Appl. Mater. Interfaces* **2017**, *9*, 345-353.

(28) Zhang, Y.; Yang, Y.; Hou, H.; Yang, X.; Chen, J.; Jing, M.; Jia, X.; Ji, X.: Enhanced Sodium Storage Behavior of Carbon Coated Anatase TiO_2 Hollow Spheres. *J. Mater. Chem. A* **2015**, *3*, 18944-18952.

(29) Chu, C.; Yang, J.; Zhang, Q.; Wang, N.; Niu, F.; Xu, X.; Yang, J.; Fan, W.; Qian, Y.: Biphase-Interface Enhanced Sodium Storage and Accelerated Charge Transfer: Flower-Like Anatase/Bronze TiO_2/C as an Advanced Anode Material for Na-Ion Batteries. *ACS Appl. Mater. Interfaces* **2017**, *9*, 43648-43656.

(30) Tao, H.; Zhou, M.; Wang, K.; Cheng, S.; Jiang, K.: Glycol Derived Carbon-$TiO_{(2)}$ as Low Cost and High Performance Anode Material for Sodium-Ion Batteries. *Sci. Rep.* **2017**, *7*, 43895.

(31) Tahir, M. N.; Oschmann, B.; Buchholz, D.; Dou, X.; Lieberwirth, I.; Panthöfer, M.; Tremel, W.; Zentel, R.; Passerini, S.: Extraordinary Performance of Carbon-Coated Anatase TiO_2 as Sodium-Ion Anode. *Adv. Energy Mater.* **2016**, *6*, 1501489.

(32) Zhang, Y.; Foster, C. W.; Banks, C. E.; Shao, L.; Hou, H.; Zou, G.; Chen, J.; Huang, Z.; Ji, X.: Graphene-Rich Wrapped Petal-Like Rutile TiO_2 tuned by Carbon Dots for High-Performance Sodium Storage. *Adv. Mater.* **2016**, *28*, 9391-9399.

(33) Wang, B.; Zhao, F.; Du, G.; Porter, S.; Liu, Y.; Zhang, P.; Cheng, Z.; Liu, H. K.; Huang, Z.: Boron-Doped Anatase TiO_2 as a High-Performance Anode Material for Sodium-Ion Batteries. *ACS Appl. Mater. Interfaces* **2016**, *8*, 16009-16015.

(34) Li, Y.-N.; Su, J.; Lv, X.-Y.; Long, Y.-F.; Yu, H.; Huang, R.-R.; Xie, Y.-C.; Wen, Y.-X.: Zn^{2+} Doped TiO_2/C with Enhanced Sodium-ion Storage Properties. *Ceram. Int.* **2017**, *43*, 10326-10332.

(35) Yan, D.; Yu, C.; Zhang, X.; Li, J.; Li, J.; Lu, T.; Pan, L.: Enhanced Electrochemical Performances of Anatase TiO_2 Nanotubes by Synergetic Doping of Ni and N for Sodium-ion Batteries. *Electrochim. Acta* **2017**, *254*, 130-139.

(36) Lai, Y.; Liu, W.; Li, J.; Zhang, K.; Qin, F.; Wang, M.; Fang, J.: High

Performance Sodium Storage of Fe-doped Mesoporous Anatase TiO_2/Amorphous Carbon Composite. *J. Alloys Compd.* **2016**, *666*, 254-261.

(37) Ni, J.; Fu, S.; Wu, C.; Maier, J.; Yu, Y.; Li, L.: Self-Supported Nanotube Arrays of Sulfur-Doped TiO_2 Enabling Ultrastable and Robust Sodium Storage. *Adv. Mater.* **2016**, *28*, 2259-2265.

(38) Hwang, J.-Y.; Myung, S.-T.; Lee, J.-H.; Abouimrane, A.; Belharouak, I.; Sun, Y.-K.: Ultrafast Sodium Storage in Anatase TiO_2 Nanoparticles Embedded on Carbon Nanotubes. *Nano Energy* **2015**, *16*, 218-226.

(39) Zhang, Y.; Wang, C.; Hou, H.; Zou, G.; Ji, X.: Nitrogen Doped/Carbon Tuning Yolk-Like TiO_2 and Its Remarkable Impact on Sodium Storage Performances. *Adv. Energy Mater.* **2017**, *7, 1600173*..

(40) Chen, C.; Wen, Y.; Hu, X.; Ji, X.; Yan, M.; Mai, L.; Hu, P.; Shan, B.; Huang, Y.: Na^+ Intercalation Pseudocapacitance in Graphene-coupled Titanium Oxide Enabling Ultra-fast Sodium Storage and Long-term Cycling. *Nat. Commun.* **2015**, *6, 6929*.

(41) Wang, L.; Xie, X.; Dinh, K. N.; Yan, Q.; Ma, J.: Synthesis, Characterizations, and Utilization of Oxygen-deficient Metal Oxides for Lithium/Sodium-ion Batteries and Supercapacitors. *Coord. Chem. Rev.* **2019**, *397*, 138-167.

(42) Le, Z.; Liu, F.; Nie, P.; Li, X.; Liu, X.; Bian, Z.; Chen, G.; Wu, H. B.; Lu, Y.: Pseudocapacitive Sodium Storage in Mesoporous Single-Crystal-like TiO_2–Graphene Nanocomposite Enables High-Performance Sodium-Ion Capacitors. *ACS Nano* **2017**, *11*, 2952-2960.

(43) Xu, G.-L.; Xiao, L.; Sheng, T.; Liu, J.; Hu, Y.-X.; Ma, T.; Amine, R.; Xie, Y.; Zhang, X.; Liu, Y.; Ren, Y.; Sun, C.-J.; Heald, S. M.; Kovacevic, J.; Sehlleier, Y. H.; Schulz, C.; Mattis, W. L.; Sun, S.-G.; Wiggers, H.; Chen, Z.; Amine, K.: Electrostatic Self-Assembly Enabling Integrated Bulk and Interfacial Sodium Storage in 3D Titania-Graphene Hybrid. *Nano Lett.* **2018**, *18*, 336-346.

(44) Zhang, H.; Jiang, Y.; Qi, Z.; Zhong, X.; Yu, Y.: Sulfur Doped Ultra-thin

Anatase TiO_2 Nanosheets/Graphene Nanocomposite for High-performance Pseudocapacitive Sodium Storage. *Energy Stor. Mater.* **2018**, *12*, 37-43.

(45) Zhang, Y.; Ding, Z.; Foster, C. W.; Banks, C. E.; Qiu, X.; Ji, X.: Oxygen Vacancies Evoked Blue TiO_2(B) Nanobelts with Efficiency Enhancement in Sodium Storage Behaviors. *Adv. Funct. Mater.* **2017**, *27*, 1700856.

(46) Oh, S. M.; Kim, I. Y.; Patil, S. B.; Park, B.; Lee, J. M.; Adpakpang, K.; Chae, S. A.; Han, O. H.; Hwang, S.-J.: Improvement of Na Ion Electrode Activity of Metal Oxide via Composite Formation with Metal Sulfide. *ACS Appl. Mater. Interfaces* **2017**, *9*, 2249-2260.

(47) Zhu, Y.; Huang, Z.; Hu, Z.; Xi, L.; Ji, X.; Liu, Y.: 3D Interconnected Ultrathin Cobalt Selenide Nanosheets as Cathode Materials for Hybrid Supercapacitors. *Electrochim. Acta* **2018**, *269*, 30-37.

(48) Saha, N. C.; Tompkins, H. G.: Titanium Nitride Oxidation Chemistry: an X-ray Photoelectron Spectroscopy Study. *J. Appl. Phys.* **1992**, *72*, 3072-3079.

(49) Li, W.; Zhou, M.; Li, H.; Wang, K.; Cheng, S.; Jiang, K.: A High Performance Sulfur-doped Disordered Carbon Anode for Sodium Ion Batteries. *Energy Environ. Sci.* **2015**, *8*, 2916-2921.

(50) Nishikiori, H.; Hayashibe, M.; Fujii, T.: Visible Light-Photocatalytic Activity of Sulfate-Doped Titanium Dioxide Prepared by the Sol-Gel Method. *Catalysts* **2013**, *3*, 363.

(51) Reddy, P. A. K.; Reddy, P. V. L.; Sharma, V. M.; Srinivas, B.; Kumari, V. D.; Subrahmanyam, M.: Photocatalytic Degradation of Isoproturon Pesticide on C, N and S Doped TiO_2. *J. water resource prot.* **2010**, *2*, 235-244.

(52) Periyat, P.; Pillai, S. C.; McCormack, D. E.; Colreavy, J.; Hinder, S. J.: Improved High-Temperature Stability and Sun-Light-Driven Photocatalytic Activity of Sulfur-Doped Anatase TiO_2. *J. Phys. Chem. C* **2008**, *112*, 7644-7652.

(53) Zhang, S.; Yao, F.; Yang, L.; Zhang, F.; Xu, S.: Sulfur-doped Mesoporous Carbon from Surfactant-intercalated Layered Double Hydroxide Precursor as High-performance Anode Nanomaterials for Both Li-ion and Na-ion Batteries.

Carbon **2015**, *93*, 143-150.

(54) Ai, W.; Luo, Z.; Jiang, J.; Zhu, J.; Du, Z.; Fan, Z.; Xie, L.; Zhang, H.; Huang, W.; Yu, T.: Nitrogen and Sulfur Codoped Graphene: Multifunctional Electrode Materials for High-Performance Li-Ion Batteries and Oxygen Reduction Reaction. *Adv. Mater.* **2014**, *26*, 6186-6192.

(55) Chen, J.; Zou, G.; Hou, H.; Zhang, Y.; Huang, Z.; Ji, X.: Pinecone-like Hierarchical Anatase TiO_2 Bonded with Carbon Enabling Ultrahigh Cycling Rates for Sodium Storage. *J. Mater. Chem. A* **2016**, *4*, 12591-12601.

(56) Korenblit, Y.; Kajdos, A.; West, W. C.; Smart, M. C.; Brandon, E. J.; Kvit, A.; Jagiello, J.; Yushin, G.: In Situ Studies of Ion Transport in Microporous Supercapacitor Electrodes at Ultralow Temperatures. *Adv. Funct. Mater.* **2012**, *22*, 1655-1662.

(57) Kiciński, W.; Szala, M.; Bystrzejewski, M.: Sulfur-doped Porous Carbons: Synthesis and Applications. *Carbon* **2014**, *68*, 1-32.

(58) Ding, S.; Chen, J. S.; Luan, D.; Boey, F. Y. C.; Madhavi, S.; Lou, X. W.: Graphene-supported Anatase TiO_2 Nanosheets for Fast Lithium Storage. *Chem. Commun.* **2011**, *47*, 5780-5782.

(59) Sun, X.; Li, Y.: Colloidal Carbon Spheres and Their Core/Shell Structures with Noble-Metal Nanoparticles. *Angew. Chem. Int. Ed.* **2004**, *43*, 597-601.

(60) Wang, B.; Xin, H.; Li, X.; Cheng, J.; Yang, G.; Nie, F.: Mesoporous CNT@TiO(2)-C Nanocable with Extremely Durable High Rate Capability for Lithium-Ion Battery Anodes. *Sci. Rep.* **2014**, *4*, 3729.

(61) Peng, G.; Ellis, J. E.; Xu, G.; Xu, X.; Star, A.: In Situ Grown TiO_2 Nanospindles Facilitate the Formation of Holey Reduced Graphene Oxide by Photodegradation. *ACS Appl. Mater. Interfaces* **2016**, *8*, 7403-7410.

(62) Wei, W.; Yang, S.; Zhou, H.; Lieberwirth, I.; Feng, X.; Müllen, K.: 3D Graphene Foams Cross-linked with Pre-encapsulated Fe_3O_4 Nanospheres for Enhanced Lithium Storage. *Adv. Mater.* **2013**, *25*, 2909-2914.

(63) Chen, W.; Li, S.; Chen, C.; Yan, L.: Self-Assembly and Embedding of

Nanoparticles by In Situ Reduced Graphene for Preparation of a 3D Graphene/Nanoparticle Aerogel. *Adv. Mater.* **2011**, *23*, 5679-5683.

(64) Wu, L.; Bresser, D.; Buchholz, D.; Giffin, G. A.; Castro, C. R.; Ochel, A.; Passerini, S.: Unfolding the Mechanism of Sodium Insertion in Anatase TiO_2 Nanoparticles. *Adv. Energy Mater.* **2015**, *5,* 1401142.

(65) Yang, X.; Wang, C.; Yang, Y.; Zhang, Y.; Jia, X.; Chen, J.; Ji, X.: Anatase TiO_2 Nanocubes for Fast and Durable Sodium Ion Battery Anodes. *J. Mater. Chem. A* **2015**, *3*, 8800-8807.

(66) Lindström, H.; Södergren, S.; Solbrand, A.; Rensmo, H.; Hjelm, J.; Hagfeldt, A.; Lindquist, S.-E.: Li+ Ion Insertion in TiO_2 (Anatase). 2. Voltammetry on Nanoporous Films. *J. Phys. Chem. B* **1997**, *101*, 7717-7722.

(67) He, X.; Jiang, J.; Tian, H.; Niu, Y.; Li, Z.; Hu, Y.; Fan, J.; Wang, C.: A Facile Method to Synthesize CoV_2O_6 as a High-performance Supercapacitor Cathode. *RSC Adv.* **2019**, *9*, 9475-9479.

TOC figure: